Predicting Gas Hydrate Formation During Three-Phase Gas-(Water-in-Oil) Flow

Carlos Lange-Bassani, Fausto A. A. Barbuto, Rigoberto E.M. Morales, Ana Cameirão, Jean-Michel Herri, Amadeu K. Sum

HAL Id: emse-02413836
https://hal-emse.ccsd.cnrs.fr/emse-02413836

Submitted on 13 Apr 2020

Predicting gas hydrate formation during three-phase gas-(water-in-oil) flow

Carlos L. Bassani, Fausto A. A. Barbuto, Rigoberto E.M. Morales
Multiphase Flow Research Center (NUEM), Federal University of Technology – Paraná (UTFPR), Rua Deputado Heitor Alencar Furtado, 5000, Bloco N, CEP 81280-340, Curitiba/PR, Brazil

Ana Cameirão, Jean-Michel Herri
Mines Saint-Etienne, Univ Lyon, CNRS, UMR 5307 LGF, Centre SPIN, Departement PEG, F - 42023 Saint-Etienne France

Amadeu K. Sum
Hydrates Energy Innovation Laboratory, Chemical and Biological Engineering Department, Colorado School of Mines, 1500 Illinois St., Golden, CO 80401, USA

Abstract. A new predictive model for hydrate formation kinetics that captures the porous structure evolution in time is coupled with a multiphase flow mechanistic model. It is assumed that the hydrate particles behave as sponges, related to hydrate formation under flow shear. The multiphase flow is considered as a gas-liquid slug flow, where the liquid is a water-in-oil emulsion. Closure parameters for the model are thoroughly discussed and the model trend is validated against experimental results obtained in a flow loop. Mass and heat transfer limitation processes are discussed in terms of the theoretical predictions from the model.
Keywords: flow assurance, gas hydrates, growth kinetics, slug flow

1 INTRODUCTION

Gas hydrates are crystals formed by the imprisonment of gas molecules in cages formed by hydrogen-bonded water molecules (1). The high pressure and low temperature conditions often found in offshore oil and gas production operations favor gas hydrate formation. The uncontrolled growth and agglomeration of these crystals can cause pipeline plugging, with production stop and related revenue losses, and thus such phenomenon is nowadays regarded as the main challenge in flow assurance (2).

Literature on equilibrium of gas hydrates is considerably developed and focused on predicting the displacement of the thermodynamic envelope of gas hydrate formation in the presence of thermodynamic inhibitors (e.g., alcohols and salts). The knowledge of the equilibrium conditions is used as a strategy for preventing hydrate formation, where hydrates are never permitted to form inside the pipeline. A more modern strategy is hydrate management, where hydrates are allowed to form as a stable slurry that is carried by the multiphase mixture up to the pipeline exit. The amount of chemical injection for avoiding particle agglomeration is much smaller than the one required to displace the hydrate formation envelope, and thus hydrate management has drawn attention from engineers, especially with the growing appearance of harsher conditions found in long tiebacks in deeper and colder waters.

There is however a lack of comprehension on the kinetics of gas hydrates growth in order to assure continuous flow. Industries use a trial-and-error process in order to understand the efficiency of Anti-Agglomerants for different flow conditions (e.g., water cut, flowrate, salt presence, oil characteristics). In parallel, science is still trying to develop a better understanding of growth kinetics and agglomeration processes.

For gas-water systems, the absorption process of gas by water; the bulk depletion due to gas consumption when hydrates form; the mass transfer between bulk and particle; and the crystal integration in the outer surface – also called intrinsic kinetics (3,4), i.e., the rate of attachment of building units in the growing surface (5) – are described (6) alongside with the population dynamics of nucleation, agglomeration and breakage of the particles (7,8). The mathematical description of gas-water-oil systems is however more complicated and still in the step of modeling growth kinetics. Most models for predicting the hydrate formation rate come from fitted Arrhenius-type correlations following Vysniauskas and Bishnoi (9). The available predictive models are for low water cut (oil-continuous flow) and are based mainly on the gas diffusion through solid shells of hydrates formed over water droplets (4,10). The evidence of the formation of this shell exists for static systems; however, for non-static systems the relative motion can make the particles form as small 'sponges' (deformable porous structure), for which the shrinkage core models are probably not well-posed, as discussed in this article.

In this study, we propose a new model to predict hydrate growth kinetics based on the assumption that particles are 'sponge-like' and that crystallization occurs mainly in the walls of the capillaries of the porous structure. The kinetic model (that predicts mass transfer limitation) is coupled with a multiphase slug flow model (11,12) in order to predict pressure and temperature variations along the pipeline, which by their turn introduce the so-called heat transfer limitation – that is, driving force variations that change the supersaturation over the growing surfaces.

2 MODEL DESCRIPTION

As shown in Figure 1, the oil-water interface is the thermodynamically favorable site for hydrate nucleation (Figure 1(a-b)) since hydrocarbon gases (in this study, methane) are more soluble in oil than in water and, therefore, supersaturation is higher at the interface. For static systems, growth will predominantly happen in the tangential direction, since axial growth would require either gas diffusion or water permeation through the formed hydrate film (Figure 1(c)). This is called heterogeneous kinetics and causes the hydrates to form as a shell encompassing the water droplets (Figure 1(d)), which is currently the hypothesis favored in the literature about gas hydrates growth kinetics in water-in-oil emulsions (4,10).

Although evidences of shell formation in static systems exist, it is highly improbable that it occurs in non-static systems, since crystal rotation and relative motion will not promote a preferential growth direction (Figure 1(e)), and the kinetics is therefore called homogeneous and a shell is not formed (Figure 1(f)). Furthermore, even if the sponge is formed, its splitting into small pieces due to flow shear is highly probable, and consequent agglomeration of those pieces into a particle without a liquid core can happen. In any case (homogeneous or heterogeneous kinetics, with or without a liquid core), the hydrate structure will be predominantly porous due to the presence of impurities, ionic forces and high driving forces (3). Since gas hydrates are hydrophilic (unless surfactants are present), the capillaries then trap water (4,13).

The growing surface is where water and gas are available near an already formed hydrate surface. In this case, it will be on the capillary walls, which trap water. Gas however needs to diffuse up to the capillaries. Even if initially the system can be considered as saturated in gas, the gas is consumed as hydrates form, triggering a mass transfer process from the gaseous free phase up to the capillaries.

Figure 2(a) presents the analyzed case of multiphase flow, considered as a gas-liquid slug flow, where the liquid is a water-in-oil emulsion. All the droplets prior to hydrate formation are considered to instantly turn into hydrate particles with the same size of the droplets. For the sake of simplification, the agglomeration process is neglected. Therefore, in order to estimate the supersaturation at the capillary walls, the following processes need to be modeled (Figure 2(b)): (i) the gas solubilization into the oil; (ii) the competition between the absorption rate of gas by the oil bulk and the depletion rate of gas due to hydrate formation; (iii) the gas mass transfer between the particle and the bulk; and (iv) the concomitant diffusion of gas through the capillaries and consumption of gas due to crystallization in the capillary walls.
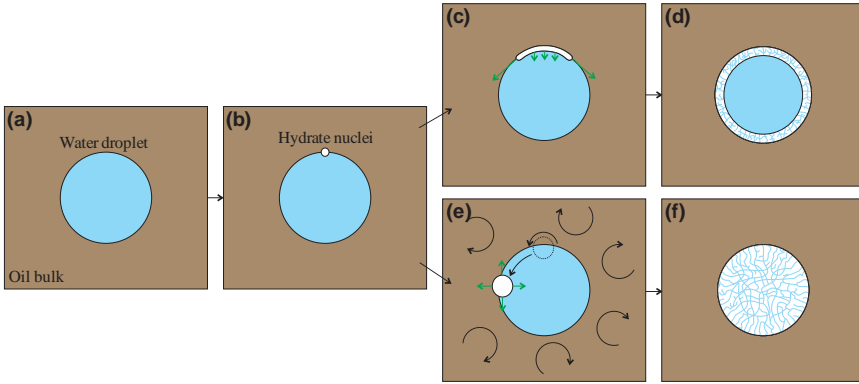
Figure 1. (a) Water droplet in oil continuous flow. (b) The preferential nucleation site is the water-oil interface. For static systems: (c) tangential growth is predominant and the kinetics is called heterogeneous; and (d) hydrates form as shells encompassing the water droplets. For non-static systems: (e) relative motion between crystal and droplet causes no preferential growth direction, called homogeneous kinetics; and (f) the shells are not formed.
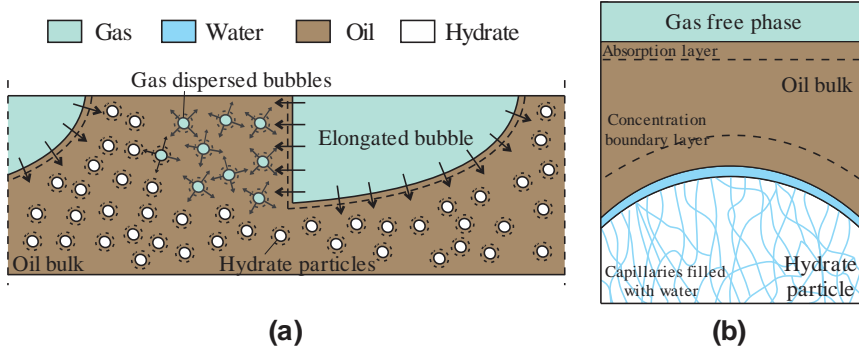

Figure 2. (a) Multiphase flow is assumed as gas-liquid slug flow, where liquid is water-in-oil emulsion. All droplets are assumed to convert to hydrate particles. (b) In order for the gas to reach the growing surfaces, it must to be absorbed by the oil, to be transferred to the outer surface of the particle, to solubilize in water, to diffuse in the water trapped in the capillaries and then to crystallize in the capillary walls.

By knowing the supersaturation in the capillaries, the gas hydrate formation rate can then be estimated. As hydrates form, heat is released to the mixture bulk and exchanged with the external medium. Temperature variations will cause different driving forces in the kinetics. As well, as crystallization on the capillary wall takes place, the capillaries fill-up, causing a reduction in the active surface for crystallization. All these phenomena must be solved together for each time step (or in each distance step, considering that as hydrates form the particles are carried away by the mixture along the pipeline assuming a steady-state flow).

2.1 Growth kinetics of gas hydrates

The growing surfaces are considered to be the capillary walls. Figure 3 presents the concomitant gas diffusion through water trapped in the capillaries and gas consumption due to crystallization. The following ODE comes from a mass balance in a differential control volume inside the capillary:

$$\frac{d^2C}{dz^2} - \frac{2k_i}{r_c D_w H_w}\left(C - H_w f_{eq}\right) = 0 \text{ with } \left.\frac{dC}{dz}\right|_{z\to\infty} = 0 \text{ and } C\big|_{\bar{z}=0} = C_{out,w} \tag{1}$$
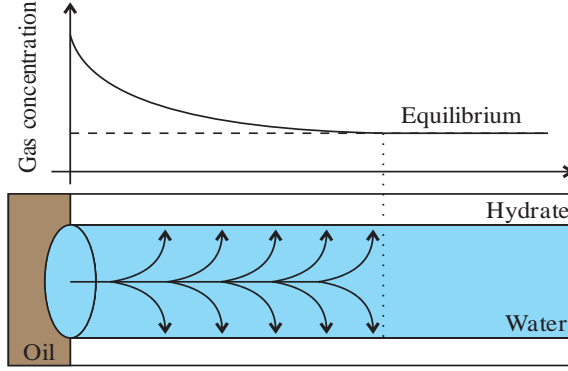
Figure 3. Competition between gas diffusion through water inside the capillaries and crystallization in the capillary walls cause a gas concentration profile along the axial direction of the capillary.

where C is the gas concentration inside the capillary, z is the axial direction of the capillaries pointing inwardly to the particle, k_i is the constant of proportionality of crystal integration using a 1st order crystallization law in terms of the fugacity difference, r_c is the capillary radius, D_w is the gas diffusivity in water, H_w is Henry's constant of gas in water, and f_{eq} is the fugacity at three-phase gas-water-hydrate equilibrium. The boundary conditions for the ODE are: (i) a semi-infinite capillary, since capillary length is expected to be much greater than its radius, with complete gas consumption for $z \rightarrow \infty$; and (ii) a given concentration $C_{out,w}$ at the capillary entrance, where '*out*' refers to the outer surface of the particle and '*w*' to the gas concentration inside the water phase.

The gas concentration in the water on the outer surface of the particle depends: (i) on the solubilization process of gas from oil to water, Eq. (2), considering the interface at equilibrium and Henry's ideality; (ii) which depends on the mass transfer between the particle and the bulk, Eq. (3); (iii) which depends on the gas concentration in the bulk C_b; (iv) which comes from the competition between the gas absorption by the bulk from the gaseous free phase *vs.* the gas consumption due to gas hydrate formation of all particles i, Eq. (4) (6,7); (v) which is linked to the gas fugacity in the free gaseous phase f_g, dependent on the system pressure and temperature and on the gas component concentration inside the gaseous phase (herein a pure gas, thus $f_g(T,P)$).

$$f_{out,o} = f_{out,w} \; \rightarrow \; C_{out,w} = \frac{H_w}{H_o} C_{out,o} \quad \text{(solubilization of gas from oil to water)} \tag{2}$$

$$-\frac{dn_{g,i}}{dt}\bigg|_{hyd} = 4\pi r_p^2 h_{m,p/b}\left(C_b - C_{out,o}\right) \quad \text{(gas mass transfer between particle and bulk)} \tag{3}$$

$$\frac{dC_b}{dt} = \underbrace{\frac{k_{g/o}A_{g/o}}{\forall_o}\left(C_{g/o} - C_b\right)}_{\substack{\text{gas absorption from the gaseous} \\ \text{free phase by the bulk}}} - \underbrace{\frac{1}{\forall_o}\sum_i \frac{dn_{g,i}}{dt}\bigg|_{hyd}}_{\substack{\text{bulk depletion due} \\ \text{to hydrate formation}}} \quad \text{with } C_{g/o} = H_o f_g \quad \text{(gas solubilization in oil)} \tag{4}$$

where $-dn_{g,i}/dt\big|_{hyd}$ is the molar consumption of gas due to hydrate formation in one particle i, r_p is the particle radius, $h_{m,p/b}$ is the mass transfer coefficient between one particle and the bulk, $k_{g/o}$ is the absorption coefficient of gas by the oil phase, $A_{g/o}$ is the interfacial surface between the gaseous free phase and the bulk, $\forall_o$ is the bulk volume (oil volume) and $C_{g/o}$ is the gas concentration at the gas-oil interface, considered at equilibrium and given in terms of the Henry's constant of gas inside oil H_o.

Solving ODE (1) to find the gas concentration profile inside the water trapped in the capillary and integrating the driving force over the surface of the capillary, the gas consumption rate due to hydrate formation in one capillary comes:

$$-\frac{dn_{g,i}}{dt}\bigg|_{1\,cap} = \frac{\pi r_c^{3/2}}{(1+\omega)}\sqrt{2H_w D_w k_i}\left(\frac{C_b}{H_o} - f_{eq}\right) \text{ with } \omega = \frac{n_c}{h_{m,p/b}}\frac{H_w}{H_o}\frac{r_c^{3/2}}{4r_p^2}\sqrt{\frac{2D_w k_i}{H_w}} \tag{5}$$

where ω represents how much mass transfer between particle and bulk limits the crystallization in the capillary walls, with $\omega \to 0$ for the case of highly agitated systems where $h_{m,p/b} \to \infty$. The number of capillaries per particle n_c evolves in time, since capillaries are filled up. Simultaneously, new capillaries are formed due to water squeezing from the 'sponge', with related cracking of the crystalline structure due to low oscillations (shear) and/or due to water compression once the capillaries fill up (since hydrates are more voluminous than the consumed water that was trapped inside the capillaries). Considering a simple birth/death population balance, and by the use of a birth rate linearly proportional to the death rate (coefficient λ_c, called birth-to-death ratio of capillaries), the evolution of the number of capillaries per particle comes:

$$n_c = n_{c,in}\exp\left[-(1-\lambda_c)\frac{t}{t_{close}}\right] \text{ with } t_{close} = \frac{1}{(C_{out,w} - H_w f_{eq})(\eta+1)}\frac{\rho_h}{M_h}\frac{H_w}{k_i}r_{c,in} \tag{6}$$

where t_{close} is the time a capillary takes to close related to the driving force in $z = 0$ estimated through the solution of ODE (1), ρ_h is the hydrate density, M_h is the hydrate molar mass and η is the hydration number. This exponential function represents the same decreasing trend of hydrate permeability/effective diffusivity due to hydrate ageing presented by Shi et al. (4) in an empirical way; however, Eq. (6) captures the influence of the driving force on the death ratio of capillaries. Since we do not model λ_c, but further use a curve fitting, we stick to a constant value, although it could vary with time.

The number of capillaries can as well be understood as a surface porosity of the particle, $\varepsilon_s = n_c r_c^2 / 4r_p^2$. Finally, the total amount of gas consumption due to hydrate formation in all particles due to consumption in all capillaries comes:

$$\frac{dn_g}{dt}\bigg|_{hyd} = n_p\frac{dn_{g,i}}{dt}\bigg|_{hyd} = n_p n_c\frac{dn_{g,i}}{dt}\bigg|_{1\,cap} \tag{7}$$

where n_p is the number of particles in the system, herein considered constant, although it can evolve in time due to nucleation, agglomeration and breakage processes in real cases (7). The number of particles in the system is considered equal to the number of water droplets before hydrate formation, herein coming from the experiments. Future coupling of agglomeration to the herein presented growth kinetics/multiphase flow model will be important to understand slurry stability and consequent plugging trends.

2.2 Multiphase flow

Before hydrate formation, water is considered to be dispersed inside the oil (water cut up to $\sim 40\%$ for low viscosity oils (14)). The water-in-oil dispersion is considered as a liquid with homogeneous properties. The gas-liquid flow pattern is considered to be slug flow and follows a mechanistic modeling (11,12,15,16). The phase fractions and region lengths of the slug flow are estimated through Taitel and Barnea model (15). The pressure and temperature distributions, Eqs. (8) to (13), come from a previous study (16) coupled with the effects of high pressure scenarios in the heat exchange (12) and the heat release due to hydrate formation (11). The main phenomena are described in the equations and the original article should be perused if the reader feels the need for further details.

$$P_{(z)} = P_{in} - \left[\underbrace{\frac{\tau_{LS}S_{LS}}{A}\frac{L_S}{L_U}}_{\substack{\text{friction in the}\\\text{slug region}}} + \underbrace{\frac{\left(\overbrace{\tau_{LB}S_{LB}}^{\text{film}} + \overbrace{\tau_{GB}S_{GB}}^{\text{bubble}} + \overbrace{\tau_i S_i}^{\text{G-L interface}} \right)}{A}\frac{L_B}{L_U}}_{\text{friction in the elongated buble region}} + \underbrace{K\rho_L \frac{\left(U_{LB} - U_T\right)^2}{2L_U}}_{\substack{\text{head loss in the}\\\text{elongated bubble rear}}} \right. z \left. + \underbrace{\left(\rho_L R_{LS} + \rho_G R_{GS}\right)\frac{L_S}{L_U} g\cos\gamma}_{\text{slug region weight}} + \underbrace{\left(\rho_L R_{LB} + \rho_G R_{GB}\right)\frac{L_B}{L_U} g\cos\gamma}_{\text{elongated bubble region weight}} \right] \tag{8}$$

$$T_{(z)} = \frac{p}{n} + \left(T_{in} - \frac{p}{n}\right)\exp\left(-\frac{n}{m}z\right) \tag{9}$$

$$m = \underbrace{\rho_m c_{P,m} A L_U U_T}_{\text{sensible heat}} \quad ; \quad n = q - \underbrace{\frac{\beta_G}{\rho_G}\left(\dot{m}_{GU} + \dot{m}_{Gz}\right)L_U \frac{dP}{dz}}_{\text{gas expansivity}} \tag{10}$$

$$p = qT_W + \underbrace{\Delta E_{hyd}M_G\left(-\left.\frac{dn_g}{dt}\right|_{hyd}\right)}_{\text{heat release due to gas hydrate formation}}$$
$$+ \underbrace{\underbrace{\tau_{LS}S_{LS}L_S U_{LS}}_{\text{slug}} + \underbrace{\tau_{LB}S_{LB}L_B U_{LB}}_{\text{film}} + \underbrace{\tau_{GB}S_{GB}L_B U_{GB}}_{\text{elongated bubble}} + \underbrace{\tau_i S_i L_B\left(U_{GB} - U_{LB}\right)}_{\text{gas-liquid interface}}}_{\text{viscous dissipation}} \tag{11}$$

$$q = \underbrace{\left(\overbrace{h_{GB}S_{GB}L_B}^{\text{elongated bubble}} + \overbrace{h_{LB}S_{LB}L_B}^{\text{film}} + \overbrace{h_{LS}S_{LS}L_S}^{\text{slug}} \right)}_{\text{heat exchange with pipeline wall}} - \underbrace{\left(\dot{m}_{Lz}c_{P,L} + \dot{m}_{Gz}c_{P,G}\right)\kappa}_{\substack{\text{heat exchange between two}\\\text{consecutive unit cells}}} \tag{12}$$

$$\kappa = \exp\left(\frac{h_{LB}S_{LB}L_B + h_{GB}S_{GB}L_B}{\rho_{mB}c_{P,m}AJ}\right) - \exp\left(-\frac{h_{LS}S_{LS}L_S}{\rho_{mS}c_{P,m}AJ}\right) \tag{13}$$

where L is the length of the slug flow regions; U is the actual velocity of the phase inside each region, with related wetted surface S, shear stress τ and heat transfer coefficient h; T_W is the wall temperature; ΔE_{hyd} is the enthalpy of formation of gas hydrates; U_T is the unit cell translational velocity; and J is the mixture superficial velocity. Indexes are 'B' for elongated bubble, 'S' for slug, 'U' for slug flow unit cell, 'G' for gas phase, 'L' for liquid phase (dispersion of water-in-oil or hydrate-in-oil) and 'i' for gas-liquid interface. The liquid properties take the hydrate fraction after hydrate formation onset into account by assuming a homogeneous model. The slurry viscosity is the exception, and is computed by a specific closure correlation (17).

3   CLOSURE PARAMETERS AND MODEL TREND VALIDATION

A major issue on the predictive models for such a complex multidisciplinary model as the one herein presented is on finding the correct closure parameters. When it comes to the slug flow model, closure for the slug flow frequency (18), the unit cell translational velocity (19) and the gas fraction in the slug body (20) are needed in order to predict the slug flow geometry using the Taitel and Barnea model (15). The main issue here is that the flow pattern transition criteria and the closure correlations are for laboratory conditions (i.e., air-water flow in small pipelines – up to 50-mm ID, 20-m length). In real scenarios, large diameters and viscous oils can significantly change the behavior of these parameters. Validation of the slug flow model against experimental data has already been published in previous articles (11,16). The following maximum percentage deviations were found: (i) ±15% for the temperature gradient; (ii) ±20% for the pressure gradient, for the gas fraction in the elongated bubble and for the lengths of the unit cell and the elongated bubble; (iii) ±35% for the mixture heat transfer coefficient; and (iv) ±60% for the slug length.

Closure of the kinetic model is even more subtle, since there are a lot of micro scale parameters that cannot be measured with the instrumentation presently available (e.g., how to track the porosity evolution of a particle that flows in a pipeline?). Other parameters are curve fitted from macro scale measurements to fit a certain model, such as the constant of proportionality of the crystal integration process, and therefore they are model-dependent parameters. That is, if there is any lack of information in the model, those parameters will represent not just the crystal integration process, but several other phenomena. This is why this parameter, in the literature, spreads over several orders of magnitude, even for the common case of methane hydrate formation in a batch reactor for water-methane systems ($k_i \approx 5.5 \times 10^{-12} - 1.8 \times 10^{-7}$ mol/(m²sPa) (6,21,22)).

In this study, we selected methane sI hydrates due to the larger availability of closure parameters in literature. We selected the values of the parameters shown in Table 1 based on the order of magnitude presented in literature. Those values, however, may not be representative of the experiments used to curve fit and validate the model. Presently, an accurate measurement of the parameters in Table 1 cannot be conducted in our laboratory facilities and further experimental efforts shall be done before the model becomes applicable, engineering-wise.

There are still two parameters to be curve fitted. The first is the death-to-birth ratio of capillaries (λ_c), which herein presents a value very close to unity. The closer to unity, the slower the porosity decreases in time, which is related to the curvature of the amount of gas consumed in time (Figure 4). This curvature also depends on the capillary radius, which herein was chosen in terms of a microscope observation of natural gas from permafrost (23). The capillary radius may not however be representative of our experiments and, therefore, infinite λ_c-curve fittings might exist depending on the capillary radius adopted.

The second curve fitted parameter is an overall efficiency of the hydrate particles that are actually interacting with the bulk (α_p). E.g., for dense systems, the hypothesis of a bulk existence or that all the outer surface is transferring mass with it is not well-posed and this overall efficiency corrects it. This parameter shows a linear trend with the amount of gas consumed. Its curve fitted value is fairly small, and such a low figure can be related to the experiments in a considerably long flowloop (~ 50-m length) related to the gas absorption interface, which occurs in a restricted section of the flow (see (24)); and to the measurement of a dense flow. Therefore, probably not all particles in the flow are actually consuming gas because they are distant from the gas-liquid interface and because they interact between themselves. Furthermore, this overall efficiency also 'corrects' the uncertainties in all closure parameters used, since in some of them only a range of the order of magnitude is known.

The model was curve fitted and validated against an experiment done using the flowloop described in Melchuna et al. (24) for deionized water, methane and Kerdane (light oil with composition from C11 to C14 (25)) at low water cut (32.25%). The characteristics of the flowloop and of the experiment are presented in Table 2. A sapphire window was inserted in the flowloop to estimate the size of water droplets before hydrate formation.

Figure 4 presents the evolution in time of the molar amount of the consumed gas. The model is capable of predicting the asymptotic trend of gas hydrate formation, related to a decrease in porosity. This is considered as a trend validation, since a fully model validation would require complete parameter evaluation.

Table 1. Closure parameters used for model validation.

Parameter	Used value
Constant of proportionality of crystal integration process	$k_i = 8 \times 10^{-8} \ \dfrac{mol}{m^2 sPa}$ (21)
Absorption coefficient multiplied by interfacial surface per unit volume	$\dfrac{k_{g/b} A_{g/b}}{\forall_b} = 1 \times 10^{-2} \ s^{-1}$ (7,26)
Mass transfer coefficient between particle and bulk	$Sh_p = 2 + 0.6 Re_p^{1/2} Sc^{1/3}$ (sphere particles) (27) $h_m = \dfrac{Sh_p D_{g/o}}{d_p}$, $Re_p = \dfrac{\rho_o U_{p/b} d_p}{\mu_o}$, $Sc = \dfrac{\mu_o}{\rho_o D_{g/o}}$ (considering highly agitated systems, with $U_{p/b} = J$)
Henry's constant of methane in water	$H_w = 1.4 \times 10^{-5} \exp\left[1600\left(\dfrac{1}{T} - \dfrac{1}{T^\circ} \right) \right] \left[\dfrac{mol}{m^3 Pa} \right]$ With: $T^\circ = 298.15\,\mathrm{K}$. Validity: $\left(\left| T^\circ - T \right| \leq 20\,\mathrm{K} \right)$ (28)
Henry's constant of methane in Kerdane	$H_o \approx 2.7 \times 10^{-4} \ \dfrac{mol}{m^3 Pa}$ (80 bar, 5°C) (26)
Properties of methane sI hydrates	$\rho_h \approx 917 \ \dfrac{kg}{m^3}$; $\Delta E_{hyd} = 53 \times 10^3$ J/mol (29) $M_h \approx 17.7 \times 10^{-3} \ \dfrac{kg}{mol}$; $\eta = 6$ (1)
Kerdane properties	$\rho_o \approx 815 \ kg/m^3$ (25); $\mu_o = 2 \times 10^{-3}$ Pa.s (Newtonian behavior, measured in rheometer for 4°C, 1 bar)
Water and methane properties	Evaluated through RefProp (30), which uses methane real behavior from (31)
Diffusivities of methane in water	$D_{g/w} = 1.2 \times 10^{-9} \ \dfrac{m^2}{s}$ ($T = 283$ K, $P = 1$ bar) (32)
Hydrate initial porosity	$\varepsilon_{sup,in} = 15\%$ (23)
Capillary radius	$r_c = 350 nm$ (23)
Birth-to-death ratio of capillaries	$1 - \lambda_c = 8 \times 10^{-6}$ (curve fitted)
Overall efficiency of the model	$\alpha_p = 2.65 \times 10^{-3}$ (curve fitted)

Table 2. Characteristics of the experiments for methane hydrate formation in a flowloop following the method presented in (24).

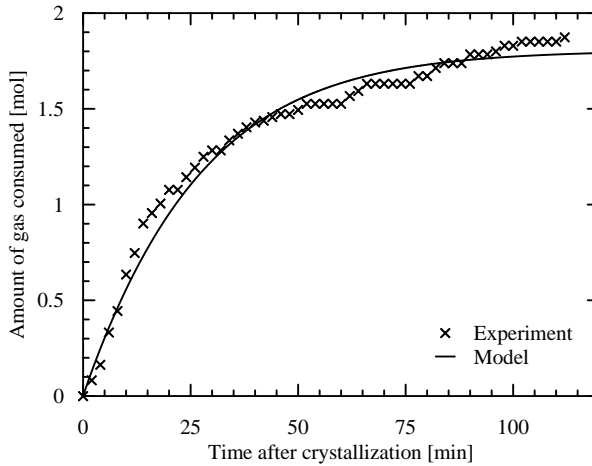|	
Fluids	Methane / Kerdane / Deionized water
Pipeline internal diameter	10.2 mm
Mixture temperature	278 K
Mixture pressure	80 bar
Mixture velocity	0.68 m/s
Water cut	32.25 %
Volume of mixture inside flowloop	10 L
Droplet diameter before hydrates onset	0.8 - 4 mm, average diameter of 2 mm

Figure 4. Model trend validation against experimental results for the molar amount of gas consumption over time.

4   RESULTS AND DISCUSSIONS

In this section we present the evaluation of the coupled model of hydrate formation kinetics with slug flow so that the heat and mass transfer limitation processes can be understood. The model input parameters are shown in

Table 3. The pipeline is considered with a small diameter (26-mm ID) due to the range of validity of the closure correlations for slug flow. The main consequence of this assumption is a significant head loss. The resulting pressure drop causes a decrease in driving force; and the consequent gas expansion increases gas superficial velocities to the point where closure correlations of the slug flow model do not behave well. Since we are interested in studying the trend behaviors of the model, simulations must form a considerable amount of gas hydrates. In this sense, we used a considerably high thermal conductivity for the pipeline wall (steel: 30 W/(m.K); thin wall: 1-mm thickness; considerable heat exchange with the environment: 100 W/(m^{2}K)). Thence, the heat transfer with the external medium is always sufficient for a heat transfer limitation not to happen (red line of Figure 5).

Table 3. Input parameters for model evaluation (coupled gas hydrate formation with slug flow).

Pipeline length / ID / width	2 km / 26 mm / 1 mm
Pipeline inclination	Horizontal
Pipeline conductivity	30 W/(m.K)
Gas superficial velocity	1 m/s
Liquid superficial velocity	1 m/s
Water cut	30%
Fluids	CH_4 / H_2O / Kerdane
Pressure at the inlet	100 bar
Temperature at the inlet	288 K
External medium temperature	277 K
External medium heat transfer coefficient	100 W/(m^{2}K)
Slug flow frequency	Schulkes (18)
Unit cell translational velocity	Bendiksen (19)
Gas fraction in the slug	Gomez et al. (20)
Slurry viscosity	Krieger and Dougherty (17)
Friction factor of the slug flow regions	Blasius (33)
Heat transfer coefficient of slug flow regions	Gnielinski (34)
Kinetic model parameters	As presented in Table 2

In this sense, a sensitivity analysis on the overall efficiency of the kinetic model was done. It is expected that the efficiency is higher than the curve fitted one for the system shown in

Table 3, since the distances from the particles to the gas-oil interfaces are smaller (in the order of magnitude of the pipeline diameter) when a free gas phase exists in the flow. An efficiency of unity means that all the particles are equally changing mass with the bulk and, consequently, with the gaseous free phase.

Figure 5 presents the results for the different overall efficiencies of the kinetic model. The dimensionless supersaturation at the capillary entrance is defined as the driving force divided by the equilibrium condition, $\bar{C}_{out,w} = \left(C_{out,w} - H_w f_{eq}\right)\big/ H_w f_{eq}$ (Figure 5(b)). Also, since an open system was simulated (differently from the closed flowloop system used to validate the kinetic model), we adhere to the analysis of the water conversion instead of the amount of gas consumed (Figure 5(d)). The trends of Figure 5 can be split into:

(A) <u>Heat transfer limited case (magenta line with stars)</u>: in this case, the external medium cannot absorb all the heat released due to gas hydrate formation and therefore the mixture reheats towards the equilibrium temperature, achieving a nearly constant subcooling (Figure 5(a)). This reheating causes the supersaturation in the capillaries to decrease (Figure 5(b)) due to: (i) increase in the three-phase hydrate-water-gas equilibrium fugacity related to the system temperature increase; and (ii) decrease in the solubility of gas inside water at higher temperatures (that is, lower solubilization in oil-water interface). With a lower gas supply, the capillary filling-up rate decreases and the porosity has a slower decrease (Figure 5(c)), and therefore the growth process lasts longer. The hydrate formation rate is nearly constant in the heat transfer limited system, and therefore the water conversion rate grows linearly (Figure 5(d)). The final attained water conversions are higher, explained by the fact that gas can penetrate deeper distances inside the capillaries since they close slower; which then incurs into a higher active surface for crystallization.

(B) <u>Mass transfer limited cases (red line with crosses and orange line with squares)</u>: the heat exchange from the mixture to the outer medium is enough to extract all the heat released due to hydrate formation and to continue to cool the mixture down further still (Figure 5(a)). Since the driving force is kept high, a considerable supersaturation is supplied in the capillaries (Figure 5(b)) and the porous structure fills up faster (Figure 5(c)). As the porosity drops down, the gas consumption rate decreases and the water conversion presents an asymptote (zoom of Figure 5(d)).

(C) <u>Competitive heat and mass transfer limitations (green line with diamonds and blue line with triangles)</u>: the heat exchange from the mixture to the outer medium extracts part of the heat released due to hydrate formation, but cannot keep cooling the mixture down (Figure 5(a)). The more the mixture reheats, the lower the driving force and the lower the supersaturation in the capillary (Figure 5(b)), incurring in a lower decrease in porosity (Figure 5(c)). When the porous structure starts to fill up, the amount of hydrate formation decreases, with a consequent decrease in heat release. Therefore, the mixture starts to cool down again (Figure 5(a)), increasing supersaturation in the capillaries (Figure 5(b)). As a rule-of-thumb, it can be said that heat transfer will mostly limit the growth process in the beginning of gas hydrate formation, where heat release is higher due to the presence of higher hydrate porosities. With time, the porous structure fills up and the process starts to be mass transfer-limited. This can be seen in the water conversion (Figure 5(d)), which presents a linear trend (heat transfer-limited, from 0.5 to ~ 1 km) that changes to a curved trend (mass transfer-limited, from ~ 1 to 2 km).

As the main conclusion from the three cases, it can be stated that heat transfer limitation causes the hydrate structure to remain 'porous' for longer time due to lower supersaturations at the growing surface. Therefore, the water tends to have a higher conversion rate for the heat transfer-limited case. Competition between the two processes depends, naturally, on the parameters used for model evaluation.
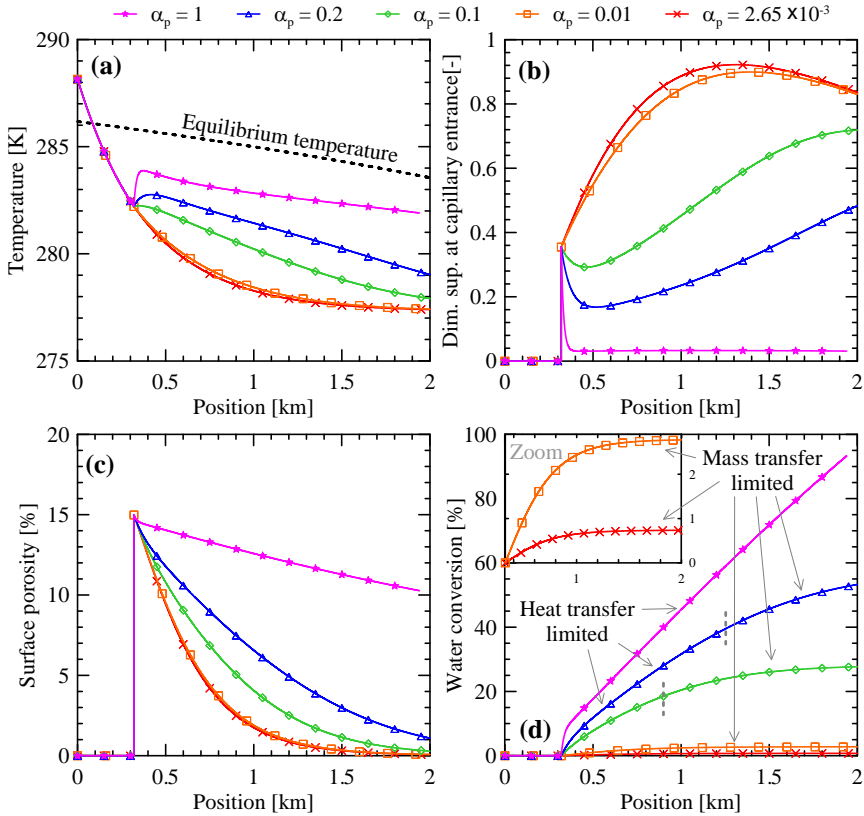
Figure 5. Evaluation for different overall efficiency of kinetic model showing heat and mass transfer limitations. Distributions along the pipeline of: (a) mixture temperature, (b) surface porosity of the particles, (c) dimensionless supersaturation at capillary entrance, and (d) water conversion.

5   CONCLUSIONS

A new hydrate formation predictive model was coupled with a slug flow model. The kinetic model includes the prediction of the evolution of the porous structure of the particles, although comparison of this evolution with experimental data was not herein presented. The lack of micro scale closure parameters for the kinetic model and macro scale closure parameters for the slug flow model in large diameter pipelines and viscous oils is still a major issue in the application of this kind of model in the industry. However, the model captures trends observed in laboratory conditions and was extended to better understand the mass and heat transfer limitations in gas hydrate formation under multiphase flow. Heat transfer limitation occurs when a high amount of capillaries (that trap water) are exposed to the oil continuous phase, thus the hydrate formation is high, with related high heat release due to the exothermic nature of gas hydrate formation. In this case, the external medium is not capable of extracting all the heat produced and the mixture reheats towards the equilibrium temperature. A smaller driving force then furnishes lower supersaturation for the capillaries to fill-up. Therefore, the structure remains 'porous' for a longer time and water conversion reaches higher levels when heat transfer initially limits hydrate formation. With time, the porous structure will close and the process will change to mass transfer-limited, seen as a change in the curvature of water conversion from linear (heat transfer-limited) to curved with an asymptote (mass transfer-limited).

REFERENCES
(1) E.D. Sloan, C.A. Koh, Clathrate hydrates of natural gases, 3rd ed., Taylor & Francis Group, Boca Raton, USA, 2008.
(2) C.A.B.R. Cardoso, M.A.L. Gonçalves, R.M.T. Camargo, Design options for avoiding hydrates in deep offshore production, J. Chem. Eng. Data. 60 (2015) 330–335. doi:dx.doi.org/10.1021/je500601f.
(3) A. Mersmann, Crystallization Technology Handbook - Second Edition Revised and Expanded, 2nd ed., Marcel Dekker Inc., New York, 2001.
(4) B.H. Shi, J. Gong, C.Y. Sun, J.K. Zhao, Y. Ding, G.J. Chen, An inward and outward natural gas hydrates growth shell model considering intrinsic kinetics, mass and heat transfer, Chem. Eng. J. 171 (2011) 1308–1316. doi:10.1016/j.cej.2011.05.029.
(5) D. Kashchiev, A. Firoozabadi, Induction time in crystallization of gas hydrates, J. Cryst. Growth. 250 (2003) 499–515. doi:10.1016/S0022-0248(02)02461-2.
(6) P. Englezos, N. Kalogerakis, P.D.D. Dholabhai, P.R.R. Bishnoi, Kinetics of formation of methane and ethane gas hydrates, Chem. Eng. Sci. 42 (1987) 2647–2658. doi:10.1016/0009-2509(87)87015-X.
(7) J.M. Herri, J.S. Pic, F. Gruy, M. Cournil, Methane hydrate crystallization mechanism from in-situ particle sizing, AIChE J. 45 (1999) 590–602.
(8) T.P. Sampaio, F.W. Tavares, P.L.C. Lage, Non-isothermal population balance model of the formation and dissociation of gas hydrates, Chem. Eng. Sci. 163 (2017) 234–254. doi:10.1016/j.ces.2016.12.012.
(9) A. Vysniauskas, P.R. Bishnoi, A kinetic study of methane hydrate formation, Chem. Eng. Sci. 38 (1983) 1061–1072. doi:10.1016/0009-2509(83)80027-X.
(10) D.J. Turner, K.T. Miller, E. Dendy Sloan, Methane hydrate formation and an inward growing shell model in water-in-oil dispersions, Chem. Eng. Sci. 64 (2009) 3996–4004. doi:10.1016/j.ces.2009.05.051.
(11) C.L. Bassani, F.A.A. Barbuto, A.K. Sum, R.E.M. Morales, A three-phase solid-liquid-gas slug flow mechanistic model coupling hydrate dispersion formation with heat and mass transfer, Chem. Eng. Sci. 178 (2018) 222–237. doi:10.1016/j.ces.2017.12.034.
(12) C.L. Bassani, F.H.G. Pereira, F.A.A. Barbuto, R.E.M. Morales, Evaluation of the gas contribution to the momentum and energy balances for liquid-gas slug flows in high pressure scenarios using a mechanistic approach, in: IV Journeys Multiph. Flows, ABCM, 2017: p. JEM-2017-0016.
(13) A. Hirata, Y.H. Mori, How liquids wet clathrate hydrates: some macroscopic observations, Chem. Eng. Sci. 53 (1998) 2641–2643. doi:10.1016/S0009-2509(98)00078-5.
(14) S. Arirachakaran, K.D. Oglesby, M.S. Malinowsky, O. Shoham, J.P. Brill, An analysis of oil/water flow phenomena in horizontal pipes, in: SPE Prod. Oper. Symp., Society of Petroleum Engineers, Oklahoma City, 1989: p. SPE-18836-MS. doi:10.2118/18836-MS.
(15) Y. Taitel, D. Barnea, A consistent approach for calculating pressure drop in inclined slug flow, Chem. Eng. Sci. 45 (1990) 1199–1206. doi:10.1016/0009-2509(90)87113-7.
(16) C.L. Bassani, F.H.G. Pereira, F.A.A. Barbuto, R.E.M. Morales, Modeling the scooping phenomenon for the heat transfer in liquid-gas horizontal slug flows, Appl. Therm. Eng. 98 (2016) 862–871. doi:10.1016/j.applthermaleng.2015.12.104.
(17) I.M. Krieger, T.J. Dougherty, A mechanism for non-newtonian flow in suspensions of rigid spheres, Trans. Soc. Rheol. 3 (1959) 137–152.
(18) R. Schulkes, Slug frequencies revisited, in: 15th Int. Conf. Multiph. Prod. Technol., BHR Group, Cannes, France, 2011: pp. 311–325.

(19) K.H. Bendiksen, An experimental investigation of the motion of long bubbles in inclined tubes, Int. J. Multiph. Flow. 10 (1984) 467–483.

(20) L.E. Gomez, O. Shoham, Y. Taitel, Prediction of slug liquid holdup: Horizontal to upward vertical flow, Int. J. Multiph. Flow. 26 (2000) 517–521. doi:10.1016/S0301-9322(99)00025-7.

(21) F.D. Al-Otaibi, Kinetic studies of gas hydrate formation using in situ particles size analysis and Raman spectroscopy, PhD Thesis, University of Calgary, 2009.

(22) S. Sharma, Gas hydrate particle size measurements, Master Thesis, University of Calgary, 1996.

(23) S.A. Klapp, S. Hemes, H. Klein, G. Bohrmann, I. MacDonald, W.F. Kuhs, Grain size measurements of natural gas hydrates, Mar. Geol. 274 (2010) 85–94. doi:10.1016/J.MARGEO.2010.03.007.

(24) A. Melchuna, A. Cameirao, J.M. Herri, P. Glenat, Topological modeling of methane hydrate crystallization from low to high water cut emulsion systems, Fluid Phase Equilib. 413 (2016) 158–169. doi:10.1016/j.fluid.2015.11.023.

(25) Total, Kerdane D 75: Safety Data Sheet, 2015.

(26) A.M. Melchuna, Experimental study and modeling of methane hydrates crystallization under flow from emulsions with variable fraction of water and anti-agglomerant, École Nationale Supérieure des Mines de Saint Étienne, 2016.

(27) R.B. Bird, W.E. Stewart, E.N. Lightfoot, Transport Phenomena, 2nd ed., John Wiley & Sons, 2002.

(28) R. Sander, Compilation of Henry's law constants (version 4.0) for water as solvent, Atmos. Chem. Phys. 15 (2015) 4399–4981. doi:10.5194/acp-15-4399-2015.

(29) J.W. Jung, D.N. Espinoza, J.C. Santamarina, Properties and phenomena relevant to CH4-CO2 replacement in hydrate-bearing sediments, J. Geophys. Res. Solid Earth. 115 (2010) B10102. doi:10.1029/2009JB000812.

(30) E.W. Lemmon, M.L. Huber, M.O. McLinden, Software: REFPROP Reference Fluid Thermodynamic and Transport Properties, 2013.

(31) U. Setzmann, W. Wagner, A New Equation of State and Tables of Thermodynamic Properties for Methane Covering the Range from the Melting Line to 625 K at Pressures up to 1000 MPa, J. Phys. Chem. Ref. Data. 20 (1991) 1061–1155. doi:10.1063/1.555898.

(32) The Engineering Toolbox, Diffusion coefficients of gases in water, (n.d.). https://www.engineeringtoolbox.com/diffusion-coefficients-d_1404.html (accessed January 17, 2019).

(33) R.W. Fox, P.J. Pritchard, A.T. McDonald, Fox and McDonald's Introduction to Fluid Mechanics, 8th ed., Sons, John Wiley &, Hoboken, USA, 2011.

(34) V. Gnielinski, New equations for heat and mass transfer in turbulent pipe and channel flow, Int. Chem. Eng. 16 (1976) 359–368.